J Comput Electron (2008) 7: 440–444
DOI 10.1007/s10825-007-0168-0

High field emission efficiency surface conduction electron emitters

Yiming Li · Hsueh-Yung Chao · Hsiang-Yu Lo

Published online: 4 January 2008

Abstract Two different surface conduction electron-emitter (SCE) structures with the nanogap of 90 nm wide fabricated by hydrogen embrittlement (HE) and focused ion beam techniques are simulated for the first time. We employ a three-dimensional particle-in-cell method coupling with finite-difference time-domain scheme to simulate the property of electron emission in these SCEs. Our calibrated simulation predicts high emission efficiency of the SCE structure which is fabricated by HE. Compared with the other SCE structure, it is observed that the proposed structure possesses low power consumption at the fixed emission current when the width of nanogap becomes narrower. The current-voltage characteristics including conducting mechanisms are investigated and explained.

Keywords Surface conduction electron-emitter · Hydrogen embrittlement · Focused ion beam · Finite-difference time-domain particle-in-cell method · Current-voltage characteristic · Electric fields · Electron trajectories

1 Introduction

Nanometer scale gaps (nanogaps) are promising for electrodes in molecular electronics [1, 2], biosensor [3], and vacuum microelectronics [4]. Researches of nanogap are only in their infancy because of the complexity and unreliability of nanogap fabrication and manipulation of nanosized constituents. One of up-to-date applications of nanogap is the surface conduction electron-emitter (SCE) for electron sources of the flat panel displays (FPDs) [5]. The surface conduction electron-emitter display (SED) is a new type of FPD based upon the SCEs. Potentiality of SCEs as field emission (FE) sources is superior to conventional cathodes in many respects. These SEDs possess high quality image, high resolution, quick response time, as well as low power consumption [5, 6], where the FE efficiency is determined by the geometry and material of SCE. As a result, the study of the structure of obtaining high emission current, high emission efficiency, and stable fabrication of SCE become one of interesting issues in recent years. The key to the SCEs at the heart of the SED is an extremely narrow fissure made from ultrafine-particle film between the two electrodes. Electrons are emitted from one side of the slit under lower driving voltage. Some of these electrons are scattered at the other side of the slit and accelerated by the high voltage applied between the anode and cathode, and they collide with the fluorescent-coated glass plate, causing light to be emitted. As shown in the previous report [7], electron trajectories in surface conduction electron-emitter display are analyzed based on the multiple scattering model. Even if this model of the electron emission mechanism of the SED has been proposed, the simulation that includes full three-dimensional (3D) fields and charged particles has not been considered for the electron emission of SED yet. Consequently, we adopt a 3D finite-difference time-domain particle-in-cell (FDTD-PIC) method in solving Maxwell equations and Lorentz equation, to simulate the electron emission in SCEs. The PIC method allows the statistical representation of general distribution functions in phase space. The use of fundamental equations often contains the full nonlinear effects, and space charge and other collective effects can be included self-consistently by coupling charged

Y. Li (✉) · H.-Y. Chao · H.-Y. Lo
Department of Communication Engineering, National Chiao Tung University, 1001 Ta Hsueh Road, Hsinchu 300, Taiwan
e-mail: ymli@faculty.nctu.edu.tw

particles to the field equations via source terms. The particle treatment permits the incorporation of relativistic effects. The PIC method retains most of the physics. Therefore, the calibrated simulation is developed to evaluate the FE property of SCE structures.

In this work, two structures of SCEs fabricated by hydrogen embrittlement (HE) [8] and focused ion beam (FIB) technique [9–12] with the separation of 90 nm wide have been investigated computationally. The calibrated model is performed by a 3D FDTD-PIC simulation for self-consistent solution of the electromagnetic fields and charged particles. We thus theoretically predict the high emission efficiency SCE structure which is fabricated by HE when the nanogap in the SCE becomes narrower. It is observed that the inclined sidewall and protrusion of this proposed SCE can function as the enhancement of the local electric fields during field emission operation and generates the high emission current at a fixed voltage. The current-voltage (I-V) characteristics, electric field distributions, conducting mechanism, and electron beam trajectories of SCE structures are discussed in this study.

2 Computational model and simulation methods

The schematic of the SCE structures is shown in Fig. 1. We first use two methods to fabricate 90 nm nanogap in the palladium (Pd) thin-film strips. One is formed by FIB technique and the other is by hydrogen embrittlement [8–12]. All process steps are compatible with contemporary integrated circuit technology. The 90 nm nanogap separation in the former method is adjusted by varying the energy of FIB, and the SEM image of nanogap is shown in Fig. 2(a). We notice that the width of the nanogaps is well controllable and about 2% variation among 9 samples of 90-nm nanogap. In the latter one, once Pd is exposed to hydrogen gas, the adsorbed hydrogen atoms can quickly diffuse into the Pd lattice and occupy the interstitial site due to a very small mass and size, and an accordingly large diffusion coefficient of hydrogen atoms. On the microscopic scale, fracture proceeds in a ductile manner which is accompanied by extensive atomic migration during the hydrogen treatment and occurs more reactive at higher temperature. The SEM image of the nanogap formed on the Pd strips in the SCE at 300 °C is shown in Fig. 2(b) with 90 nm wide.

We first formulate a calibrated model with the experimental data by using the numerical simulation [10–12]. The computational flowchart of FDTD-PIC simulation is shown in Fig. 3. The fundamentals of PIC are briefly described [13]; starting from a specified initial state, we simulate electrostatic fields as its evolution in time. We then perform a time integration of Faraday's law, Ampere's law, and the relativistic Lorentz equation, subject to constraints provided by Gauss's law and the rule of divergence of magnetic field. The full set of Maxwell equations is simultaneously solved to obtain electromagnetic fields. Similarly, the Lorentz force equation is solved to obtain relativistic particle trajectories. In addition, the electromagnetic fields are advanced in time at each time step. The charged particles are moved according to the Lorentz equation using the fields advanced in each time step. The weighted charge density and current density at the grids are subsequently calculated. The obtained charge density and current density are successively used as sources in the 3D Maxwell equations for advancing the electromagnetic fields. These steps are repeated for each time step until the specified number of time steps is reached. This 3D FDTD-PIC method thus approaches to self-consistent simulation of the electromagnetic fields and charged particles.

In the FE process, the electron emission is modeled by the Fowler-Nordheim (F-N) equation, as expressed in the inset of Fig. 3(b), where A and B are fitting parameters to be calibrated with measured data, E is the normal component of the electric field at the emitter surface, ϕ is the work function of the emission material, t^2 is approximately equal to 1.1, and $v(y) = 0.95 - y^2$ with $y = 3.79 \times 10^{-5} \times E^{1/2}/\phi$ is in SI unit. The emission current density is determined by the F-N equation according to the local electric field, the work function of emitter material, and the geometric factors. We notice that all dimensions of physical quantities are the same with the experimental settings and the surfaces in the SCE are assumed to be smooth on the cell level in the entire simulation.

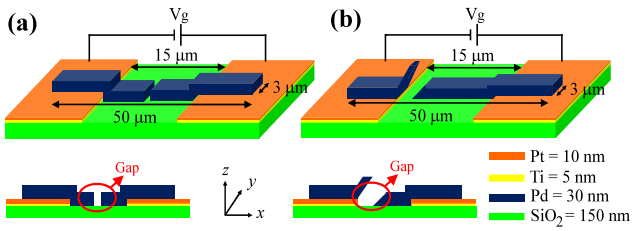

Fig. 1 A schematic plot of the SCE structures and the cross sections of the SCEs on the xz plane. The nanogap in (**a**) is formed by FIB technique and (**b**) is fabricated by hydrogen embrittlement

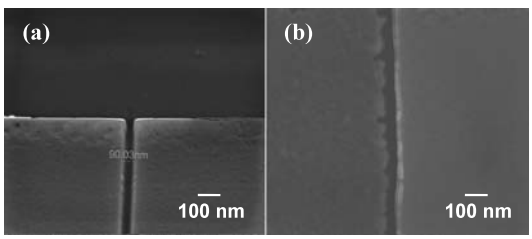

Fig. 2 The SEM images of the nanogaps formed on the Pd strips, where (**a**) is prepared by FIB technique and (**b**) is by hydrogen embrittlement. The width of nanogap is approximately 90 nm [8–12]

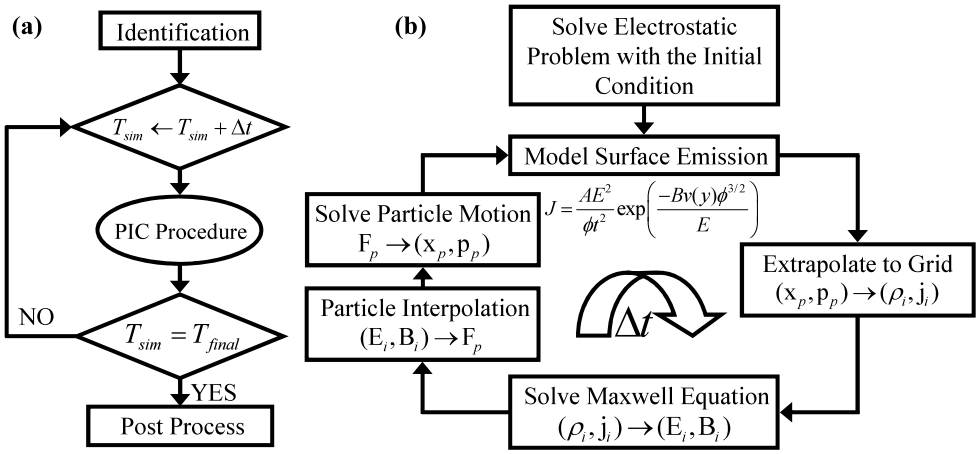

Fig. 3 (**a**) The computational scheme and (**b**) flowchart of PIC procedure for the 3D simulation

3 Results and discussion

According to the calibrated model and the experimental data [8–12], Fig. 4 shows the current-voltage (I-V) characteristics for the sample with 90 nm nanogap by two fabricated methods, where the *Vg* varies from 0 V to 300 V. The solid line indicates the data of FIB technique, the dashed-line is the HE results, and symbols are calibrated data. As the emission current attain to 0.1 mA, we find the voltage requires 160 V for the FIB technique fabricated 90 nm nanogap and 200 V in the 90 nm nanogap by the hydrogen embrittlement.

The validated model is thus extended to predict smaller size of nanogaps. We find the SCE by HE has better emission efficiency than the coplanar structure by FIB in narrower cases. For $Vg = 60$ V, it has the similar electric fields, shown in Fig. 5(a), distributed on the emitter surface to Fig. 5(b), thus the similar emission current is observed when $Vg = 60$ V, as shown in Fig. 4. However, the electric field in Fig. 5(d) is stronger than Fig. 5(c) of the case of 30 nm. We thus predict the emission current, as shown in Fig. 5(d), is higher than Fig. 5(c) in 30 nm SCE, when $Vg = 60$ V.

Figure 6 shows the simulated electron trajectories of two structures with the 90 nm and 30 nm gaps. It can clearly observe the electron-emission mechanisms. In additional, the figures are zoom-in plots around the emitter and electrons will end in the Pd strip. Figure 7(a) shows the predicted I-V characteristics for the sample with the 30 nm nanogaps, where *Vg* varies from 0 V to 100 V. It shows when the emission current get to 0.1 mA, the gate voltage in the structure by HE needs 50 V which is lower than 60 V of the SCE by FIB. Comparison among Figs. 5(c), 5(d), and Fig. 7(a) confirms the prediction. We find that the proposed structure truly possesses the high electron emission efficiency in narrower nanogaps. Figure 7(b) shows the corresponding F-N plot of the field emission of Pd SCEs. The linear relationship indicates that the electron conduction followed the F-N field emission mechanism.

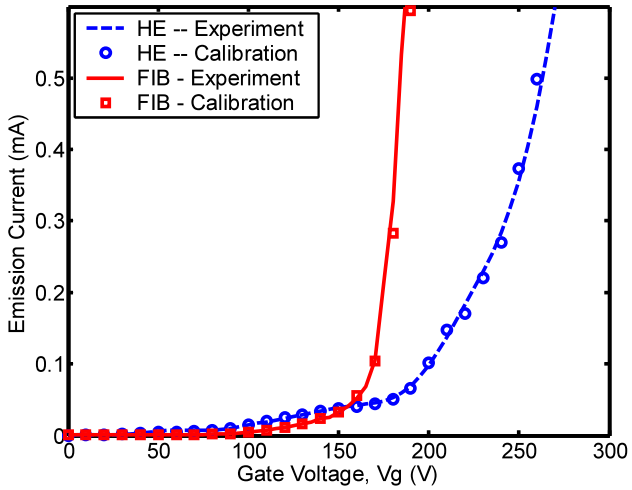

Fig. 4 The I-V characteristics of the SCE devices with 90 nm nanogap

Table 1 The gate voltages in different widths of nanogaps (extracted from the emission current > 0.1 mA)

Method	Width		
	30 nm	60 nm	90 nm
FIB	60 V	85 V	160 V
HE	50 V	80 V	200 V

4 Conclusions

In this study, we have analyzed the structure fabricated by HE technique. The result exhibits that the examined sample has high performance of field emission when it is with the 30 nm nanogap. The gate voltages are summarized in Table 1 for the emission current > 0.1 mA. We stress that the sample fabricated with simple process not only has improved FE property but also promises the advanced design of SCEs for SED technology.

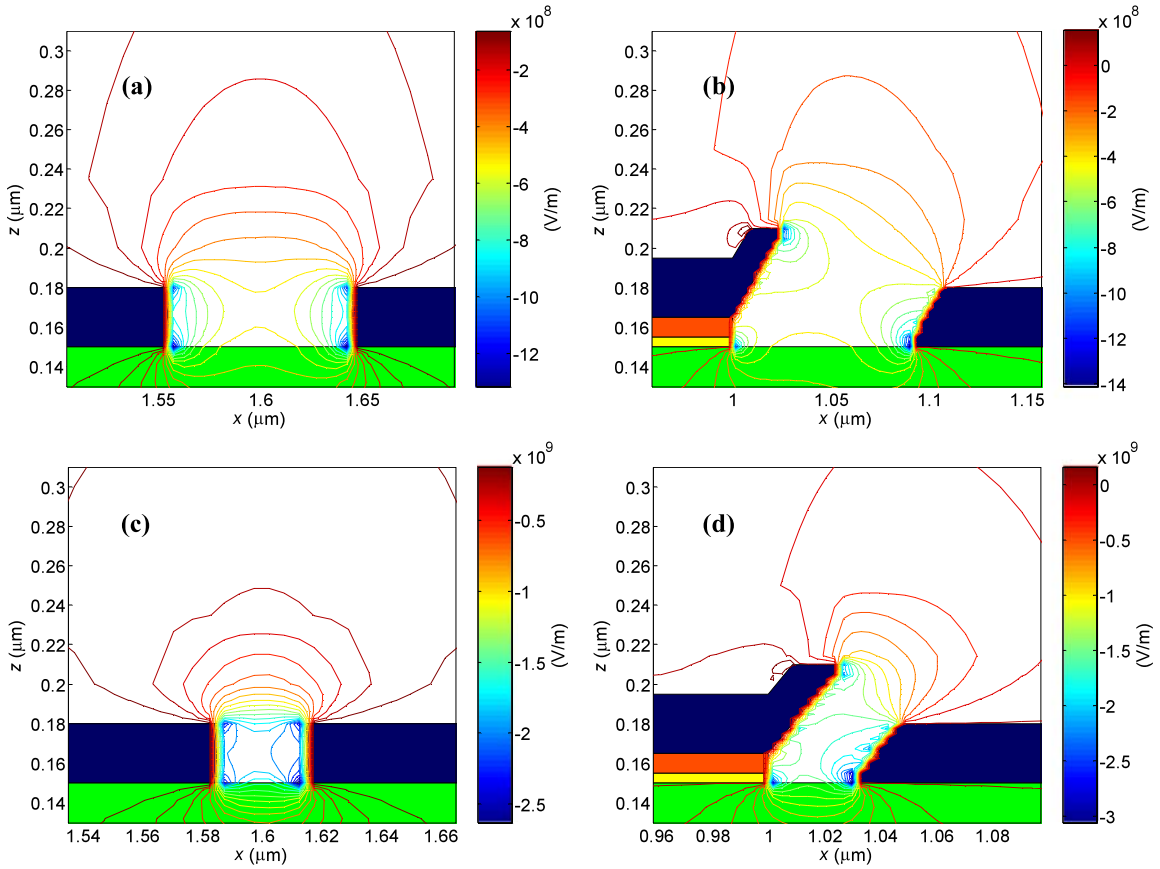

Fig. 5 The contour plots of electric fields around the emitters, where $Vg = 60$ V. (**a**) and (**c**) indicate the nanogaps formed by FIB. Nanogaps of (**b**) and (**d**) are fabricated by HE with 90 nm and 30 nm

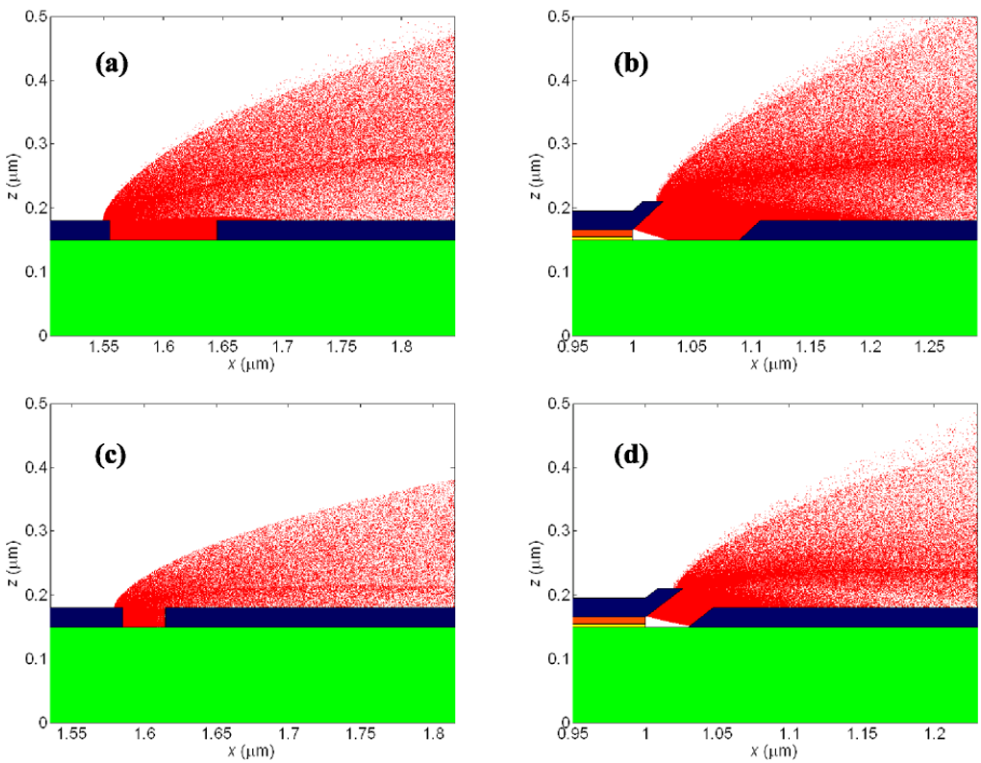

Fig. 6 The electron-beam trajectories ejected from the SCE on the *xz* plane with $Vg = 60$ V

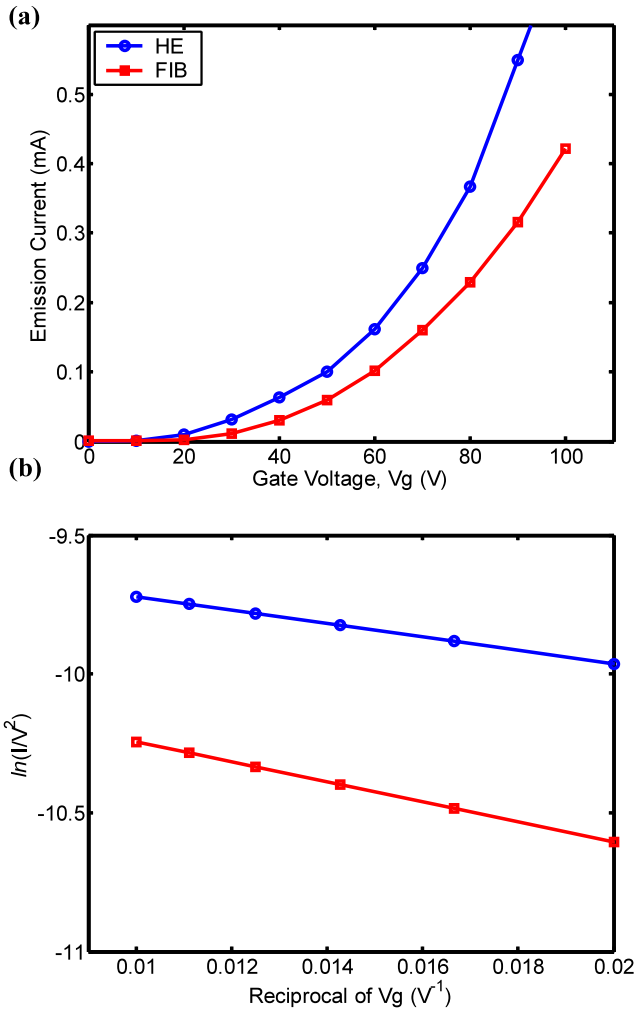

Fig. 7 Characterization of the electron emission process of SCEs with nanogap of 30 nm wide. (**a**) The I-V curves of two SCE devices. (**b**) The corresponding F-N plots

Acknowledgements This work was supported in part by Taiwan National Science Council (NSC) under NSC-96-2221-E-009-210 and Contract NSC-96-2752-E-009-003-PAE, and by the ChungHwa Picture Tubes, Ltd, under a 2006–2008 grant. The authors thank Prof. F.-M. Pan for supporting sample characterization and helpful discussion.

References

1. Reed, M.A., et al.: Conductance of a molecular junction. Science **278**, 252 (1997)
2. Linag, W., et al.: Kondo resonance in a single-molecule transistor. Nature **417**, 725 (2002)
3. Yi, M., et al.: Theoretical and experimental study towards a nanogap dielectric biosensor. Biosens. Bioelectron. **20**, 1320 (2004)
4. Lee, H.I., et al.: Nanometer-scale gap control for low voltage and high current operation of field emission array. J. Vac. Sci. Technol. B **16**, 762 (1998)
5. Sakai, K. et al.: Flat-panel displays based on surface-conduction electron emitters. In: Proc. of EuroDisplay '96, pp569 (1996)
6. Yamaguchi, E., et al.: A 10-in. surface-conduction electron-emitter display. J. SID **5**, 345 (1997)
7. Okuda, M. et al.: Electron trajectory analysis of surface conduction electron emitter displays (SEDs). In: SID '98 DIGEST, vol. 14.1, p. 185 (1998)
8. Tsai, C.H., et al.: Nanogap formation by palladium hydrogenation for surface conduction electron emitters fabrications. Appl. Phys. Lett. **90**, 163115 (2007)
9. Tsai, C.H., et al.: Nanogap fabrication on palladium electrodes for field emission display applications. SID Symp. Dig. **38**, 583 (2007)
10. Lo, H.Y., et al.: Three-dimensional simulation of novel surface conduction electron-emitters. SID Symp. Dig. **38**, 586 (2007)
11. Lo, H.Y. et al.: Experimental and theoretical examination of field emission in surface conduction electron-emitter displays. In: Extended Abstract of the 2007 International Conference on Solid State Devices and Materials, p. 544 (2007)
12. Lo, H.Y. et al.: Effect of process variation on field emission characteristic in surface conduction electron-emitters. In: Proceedings of the 7th IEEE International Conference on Nanotechnology, p. 353 (2007)
13. Birdsall, C.K., Langdon, A.B.: Plasma Physics via Computer Simulation. McGraw-Hill, New York (1985)